AIAA AVIATION Forum
June 15-19, 2020, VIRTUAL EVENT
AIAA AVIATION 2020 FORUM

10.2514/6.2020-2666

Study of Reynolds Number Effect for Co-Flow Jet Airfoil/Wing

Yang Wang * Gecheng Zha †
Dept. of Mechanical and Aerospace Engineering
University of Miami, Coral Gables, Florida 33124
E-mail: gzha@miami.edu

Abstract

This paper numerically studies the Reynolds number effect for a 2D Co-Flow Jet (CFJ) airfoil and a 3D wing at freestream Mach number of 0.46. The Reynolds averaged Navier-Stokes equations solver with Spalart-Allmaras one-equation turbulence model is utilized for the simulation. The Reynolds number is decreased from 4.1×10^6 to 0.18×10^6 to mimic the altitude change from 10000m to 30000m. The results show that, at Reynolds number of 4.1×10^6, the best CFJ airfoil corrected aerodynamic efficiency ($(C_L/C_D)_c$) of 81.64 occurs at C_μ of 0.03 at AoA of 6°. When the Reynolds number is reduced to 0.18×10^6, the $(C_L/C_D)_c$ has a 39.5% decrease. It is because of the dramatic increase of the viscous drag by 66.2%. However, the lift coefficient drops only by 5.1%. The second reason for the decrease of the CFJ airfoil corrected aerodynamic efficiency is that the power coefficient Pc is increased significantly by 85% with the decrease of the Reynolds number. It is caused mostly by the increased total pressure ratio of CFJ pumping due to higher loss. The 3D wing with an aspect ratio of 20 based on the same 2D airfoil is also studied for the same Reynolds numbers and freestream Mach number. Similar to the 2D cases, the wing at low Reynolds number suffers significantly increased viscous drag and energy loss of the CFJ.

Nomenclature

CFJ	Co-flow jet
AoA	Angle of attack
LE	Leading Edge
TE	Trailing Edge
S	Planform area
c	Airfoil chord
U	Flow velocity
q	Dynamic pressure $0.5\,\rho\,U^2$
p	Static pressure
η	Pump efficiency
ρ	Air density
$\dot{m}$	Mass flow
M	Mach number
ω	Pitching Moment

* Graduate Student
† Professor, ASME Fellow, AIAA associate Fellow

P	Pumping power
∞	Free stream conditions
$_j$	Jet conditions
C_L	Lift coefficient $L/(q_\infty S)$
C_D	Drag coefficient $D/(q_\infty S)$
C_M	Moment coefficient
C_μ	Jet momentum coef. $\dot{m}_j U_j/(q_\infty S)$
$(C_L/C_D)_c$	CFJ airfoil corrected aerodynamic efficiency $L/(D + P/V_\infty)$
Pc	Power coefficient $L/(q_\infty S V_\infty)$
PR	Total pressure ratio between injection and suction
M_{is}	Isentropic Mach Number
M_∞	Freestream Mach Number
P_{tinj}	Total injection pressure
P_{tsuc}	Total suction pressure
Re	Reynolds Number
V_{inj}	Normalized injection velocity

1 Introduction

Low Reynolds number airfoil performance is important for various applications [1], including high altitude long endurance aircraft, wind turbines, Martian aerial vehicles, etc. A Reynolds number below 10^6 is considered as the range of the low Reynolds number. The airfoil performance with the Reynolds number between 100,000 and 500,000 is in particular not well studied [1]. The flow on the suction surface (upper surface) tends to have laminar flow separation bubbles and turbulent reattachment, which deteriorates the boundary layer, decreases the L/D, creates the unsteadiness with hysteresis, and substantially reduces the airfoil operation range.

Recently, the Co-Flow Jet (CFJ) active flow control airfoil developed by Zha et al. [2, 3, 4, 5, 6, 7, 8, 9, 10, 11, 12, 13] provides a promising concept to increase maximum lift coefficient, stall AoA, and cruise efficiency at low AoA. In a CFJ airfoil, an injection slot near the leading edge (LE) and a suction slot near the trailing edge (TE) on the airfoil suction surface are created. As shown in Fig. 1, a small amount of mass flow is drawn into the suction duct, pressurized and energized by the micro compressor, and then injected near the LE tangentially to the main flow via an injection duct. The whole process does not add any mass flow to the system and hence is a zero-net-mass-flux(ZNMF) flow control. The CFJ airfoil is demonstrated to achieve radical lift augmentation, stall margin increase, drag reduction and moderate nose-down moment for stationary and pitching airfoils.

The CFJ airfoil has a unique low energy expenditure mechanism, because the jet gets injected at the leading edge peak suction location, where the main flow pressure is the lowest and makes it easy to inject the flow, and it gets sucked at the trailing edge, where the main flow pressure is the highest and makes it easy to draw the flow. The low energy expenditure is a key factor enabling the CFJ airfoil to achieve ultra-high cruise efficiency [14] at low AoA when the flow is benign.

Even though the CFJ active flow control is not specially aimed at low Reynolds number airfoil, the injection jet mixing at near leading edge appears to force the boundary layer transition to turbulent via large vortex structures [15] and avoid the major low Reynolds number airfoil problems. The three wind tunnel tests by Zha and his team have the Reynolds number of 0.38×10^6 [5], 0.2×10^6 [15], and $0.2 - 0.7 \times 10^6$ [16] respectively. They are all in the range of low Reynolds number flow. No obvious unsteadiness due to low Reynolds airfoil behaviors are observed

in the experiments. Since those studies are not specially designed to investigate low Reynolds number airfoil, it may be inclusive to claim that CFJ airfoil has no problems for low Reynolds number flows. However, in this paper we do assume the claim is true and simulate the flow with RANS model with full truculent boundary layer with no laminar to transition modeling.

The purpose of this paper is to investigate the performance of the CFJ airfoil with the Reynolds number reduced from 4.1×10^6 to 0.18×10^6 to mimic the effect of altitude change from 10000m to 30000m. Both 2D airfoil and 3D wing are simulated at a freestream Mach number of 0.46 with different Reynolds number.

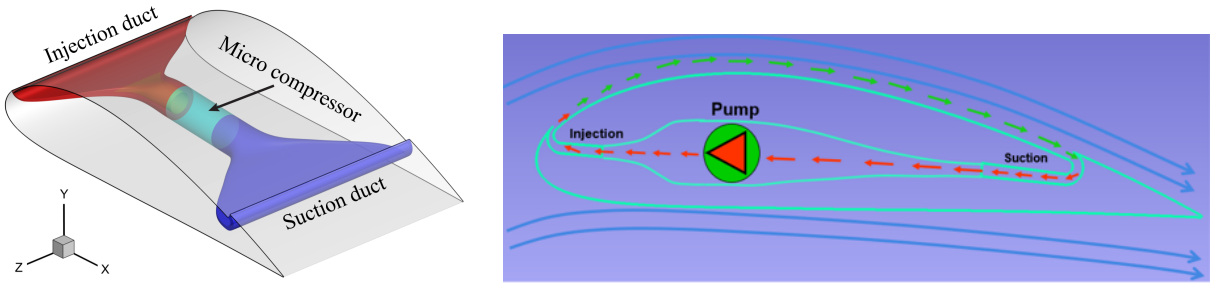

Figure 1: Schematic plot of a typical CFJ airfoil.

2 Methodology

2.1 Lift and Drag Calculation

The momentum and pressure at the injection and suction slots produce a reactionary force, which is automatically measured by the force balance in wind tunnel testing. However, for CFD simulation, the full reactionary force needs to be included. Using control volume analysis as shown in Fig. 2, the reactionary force can be calculated using the flow parameters at the injection and suction slot opening surfaces. Zha et al. [3] give the following formulations to calculate the lift and drag due to the jet reactionary force for a CFJ airfoil. By considering the effects of injection and suction jets on the CFJ airfoil, the expressions for these reactionary forces are given as :

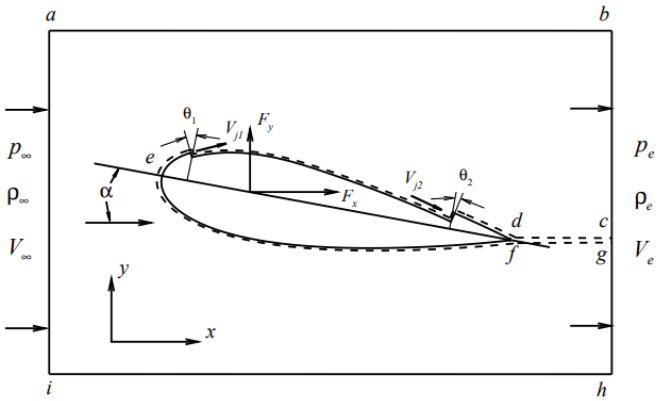

Figure 2: The control volume for a CFJ airfoil.

$$F_{x_{cfj}} = (\dot{m}_j V_{j1} + p_{j1} A_{j1}) * cos(\theta_1 - \alpha) - (\dot{m}_j V_{j2} + p_{j2} A_{j2}) * cos(\theta_2 + \alpha) \tag{1}$$

$$F_{y_{cfj}} = (\dot{m}_{j1} V_{j1} + p_{j1} A_{j1}) * sin(\theta_1 - \alpha) + (\dot{m}_{j2} V_{j2} + p_{j2} A_{j2}) * sin(\theta_2 + \alpha) \tag{2}$$

where the subscripts 1 and 2 stand for the injection and suction respectively, and θ_1 and θ_2 are the angles between the injection and suction slot's surface and a line normal to the airfoil chord. α is the angle of attack.

The total lift and drag on the airfoil can then be expressed as:

$$D = R'_x - F_{x_{cfj}} \tag{3}$$

$$L = R'_y - F_{y_{cfj}} \tag{4}$$

where R'_x and R'_y are the surface integral of pressure and shear stress in x (drag) and y (lift) direction excluding the internal ducts of injection and suction. For CFJ wing simulations, the total lift and drag are calculated by integrating Eq. (3) and Eq. (4) in the spanwise direction.

2.2 Jet Momentum Coefficient

The jet momentum coefficient C_μ is a parameter used to quantify the jet intensity. It is defined as:

$$C_\mu = \frac{\dot{m} V_j}{\frac{1}{2}\rho_\infty {V_\infty}^2 S} \tag{5}$$

where $\dot{m}$ is the injection mass flow, V_j is the mass-averaged injection velocity, ρ_∞ and V_∞ denote the free stream density and velocity, and S is the planform area.

2.3 Power Coefficient

CFJ is implemented by mounting a pumping system inside the wing that withdraws air from the suction slot and blows it into the injection slot. The power consumption is determined by the jet mass flow and total enthalpy change as the following:

$$P = \dot{m}(H_{t1} - H_{t2}) \tag{6}$$

where H_{t1} and H_{t2} are the mass-averaged total enthalpy in the injection cavity and suction cavity respectively, P is the Power required by the pump and $\dot{m}$ the jet mass flow rate. Introducing P_{t1} and P_{t2} the mass-averaged total pressure in the injection and suction cavity respectively, the pump efficiency η, and the total pressure ratio of the pump $\Gamma = \frac{P_{t1}}{P_{t2}}$, the power consumption is expressed as:

$$P = \frac{\dot{m} C_p T_{t2}}{\eta} (\Gamma^{\frac{\gamma-1}{\gamma}} - 1) \tag{7}$$

where γ is the specific heat ratio equal to 1.4 for air. The power coefficient is expressed as:

$$P_c = \frac{P}{\frac{1}{2}\rho_\infty V_\infty^3 S} \tag{8}$$

2.4 Corrected Aerodynamic Efficiency

The conventional wing aerodynamic efficiency is defined as:

$$\frac{L}{D} \tag{9}$$

For the CFJ wing, the ratio above still represents the pure aerodynamic relationship between lift and drag. However since CFJ active flow control consumes energy, the ratio above is modified to take into account the energy consumption of the pump. The formulation of the corrected aerodynamic efficiency for CFJ wings is:

$$(\frac{L}{D})_c = \frac{C_L}{C_D + P_c} \tag{10}$$

where V_∞ is the free stream velocity, P is the pumping power, and L and D are the lift and drag generated by the CFJ wing. The formulation above converts the power consumed by the CFJ into a force $\frac{P}{V_\infty}$ which is added to the aerodynamic drag D. If the pumping power is set to 0, this formulation returns to the aerodynamic efficiency of a conventional wing.

2.5 Aircraft Productivity

To compare aircraft that have the same ratio of initial weight to final weight with the same engine fuel consumption or battery energy density, the productivity efficiency C_L^2/C_D is introduced to measure the productivity of an airplane represented by its range multiplied by its weight [17].

The productivity efficiency $C_L^2/C_D = C_L(C_L/C_D)$ is a more comprehensive parameter than the conventional aerodynamic efficiency C_L/C_D to measure the merit of an airplane aerodynamic design for cruise performance. The former includes not only the information of C_L/C_D, but also the information of the aircraft weight C_L. For example, for two airplane designs having the same C_L/C_D with one C_L twice larger than the other, if the wing sizes are the same, one airplane will be able to carry twice more weight than the other with productivity and wing loading increased by 100%. Such a large difference is not reflected by C_L/C_D, but very well reflected by C_L^2/C_D.

The definition of C_L/C_D in general is a suitable measure of merit for conventional aircraft design. This is because at a certain Mach number regime, the maximum C_L/C_D is usually achieved at low angle of attack within the drag bucket and is more or less the same for different airfoil designs. In other words, for the same optimum C_L/C_D, the C_L is about the same. A typical C_L for subsonic airfoil is about 0.4 and for transonic airfoil is about 0.7.

For CFJ airfoil, the minimum CFJ pumping power occurs at a fairly high AoA [8, 15]. With the augmentation of CFJ, the subsonic cruise lift coefficient of a CFJ airfoil is typically 2 to 3 times higher than the conventional airfoil with about the same $(C_L/C_D)_c$ [13]. Such a high lift coefficient is unattainable for conventional airfoil since

they would be either stalled or near stalled with very high drag. Hence for CFJ aircraft design, the productivity efficiency $C_L^2/C_D = C_L(C_L/C_D)$ is more informative to be used to reflect the aerodynamic performance. The corrected productivity efficiency for CFJ airfoils is $(C_L^2/C_D)_c = C_L^2/(C_D + P_c)$.

2.6 CFD Simulation Setup

The FASIP (Flow-Acoustics-Structure Interaction Package) CFD code is used to conduct the numerical simulation. The 3D Reynolds Averaged Navier-Stokes (RANS) equations with one-equation Spalart-Allmaras [18] turbulence model is used. A 3rd order WENO scheme for the inviscid flux [19, 20, 21, 22, 23, 24] and a 2nd order central differencing for the viscous terms [19, 23] are employed to discretize the Navier-Stokes equations. The low diffusion E-CUSP scheme used as the approximate Riemann solver suggested by Zha et al [20] is utilized with the WENO scheme to evaluate the inviscid fluxes. Implicit time marching method using Gauss-Seidel line relaxation is used to achieve a fast convergence rate [25]. Parallel computing is implemented to save wall clock simulation time [26].

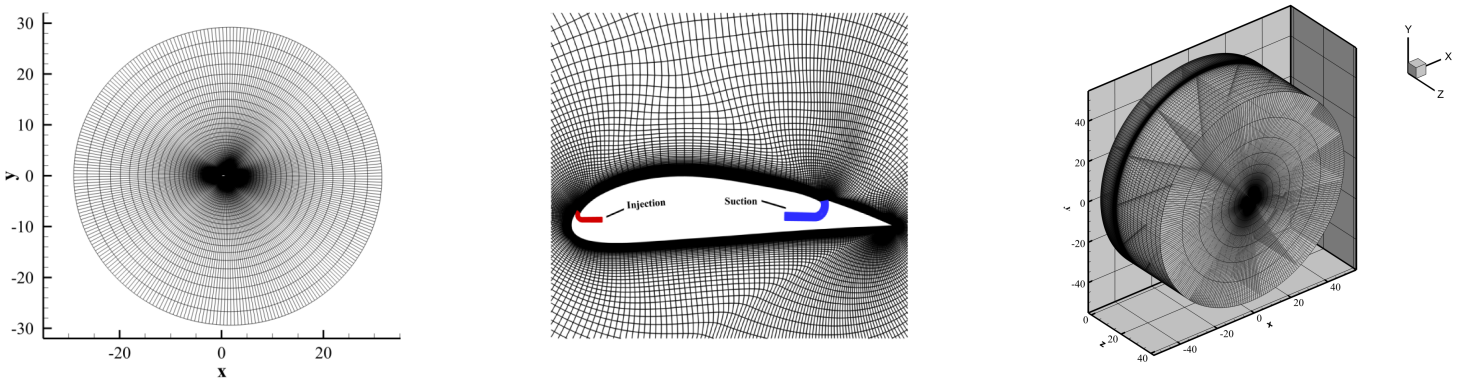

Figure 3: Computational mesh used in the current work.

2.7 Boundary Conditions

The 3rd order accuracy no slip condition is enforced on the solid surface with the wall treatment suggested in [27] to achieve the flux conservation on the wall. The computational mesh is shown in Fig. 3. The ducts geometries are predetermined according to our previous designs. Total pressure, total temperature and flow angles are specified at the injection duct inlet, as well as the upstream portion of the far field. Constant static pressure is applied at the suction duct outlet as well as the downstream portion of the far field. The total mesh size is 47,200 points, split into 10 domains for the parallel computation. The first grid point on the wing surface is placed at $y^+ \approx 1$.

3 Airfoil Geometry Parameters

Table. 1 gives the detailed parameters of CFJ6421 airfoils with the injection and suction slot size normalized by airfoil chord length (C). The CFJ6421-SST150-SUC247-INJ117 airfoil is optimized by Wang and Zha for its high

lift and cruise efficiency [28, 29, 30]. The CFJ6421-SST150-SUC247-INJ117 airfoil has a larger injection slot size of 1.17%C and suction slot size of 2.47%. The suction surface translation (SST) of 1.50%C is the same as that of CFJ6421-SST150-SUC133-INJ065 airfoil.

Table 1: Airfoil geometry parameters

Airfoil	SST (%C)	INJ (%C)	SUC (%C)
CFJ6421-SST150-SUC247-INJ117	1.50	1.17	2.47

4 Simulated Cases

Table. 2 lists all the freestream conditions and the CFJ momentum coefficients that are studied. Since the focus is on the cruise performance, the AoA is limited to low value of 0° - 14°.

Table 2: Simulation cases used in the current work

Cases	Re	AoA	C_μ
1	4.1×10^6	0°-14°	0.01 - 0.05
2	2.6×10^6	0°-14°	0.01 - 0.05
3	0.18×10^6	0°-14°	0.01 - 0.05

5 2D CFJ Airfoils at Different Reynolds Number

Table. 3, Table. 4 and Table. 5 list the 2D CFJ airfoil optimum aerodynamic efficiency at different C_μ. For all different Reynolds numbers, the optimum corrected aerodynamic efficiency ($(C_L/C_D)_c$) is at C_μ of 0.03 and AoA around 6°.

Table 3: Airfoil performance at different C_μ for CFJ airfoil with Reynolds number of 4.1×10^6.

C_μ	C_L	C_D	C_L/C_D	$(C_L/C_D)_c$	$({C_L}^2/C_D)_c$	AoA	Pc
0.01	1.0271	0.0107	95.762	74.689	76.713	2°	0.00303
0.02	1.1604	0.0078	149.708	73.991	85.859	5°	0.00969
0.03	1.7041	0.0122	139.689	81.644	139.129	6°	0.00867
0.04	1.7963	0.0101	178.583	75.788	136.136	6°	0.01377
0.05	1.8443	0.0092	201.004	64.933	119.756	6°	0.01923

Table 4: Airfoil performance at different C_μ for CFJ airfoil with Reynolds number of 2.6×10^6.

C_μ	C_L	C_D	C_L/C_D	$(C_L/C_D)_c$	$(C_L{}^2/C_D)_c$	AoA	Pc
0.01	1.0211	0.0113	90.668	70.538	72.028	2°	0.00321
0.02	1.1553	0.0082	141.301	70.111	80.999	6°	0.00830
0.03	1.5922	0.0105	132.489	77.186	122.894	5°	0.01015
0.04	1.7894	0.0104	171.440	72.044	128.913	6°	0.01440
0.05	1.8419	0.0094	196.940	62.269	114.692	6°	0.02023

Table 5: Airfoil performance at different C_μ for CFJ airfoil with Reynolds number of $0.18\times^6$.

C_μ	C_L	C_D	C_L/C_D	$(C_L/C_D)_c$	$(C_L{}^2/C_D)_c$	AoA	Pc
0.01	0.9651	0.0160	60.286	44.732	43.170	2°	0.00557
0.02	1.3883	0.0186	74.753	49.125	68.201	5°	0.00969
0.03	1.6172	0.0167	96.767	49.382	79.859	6°	0.01603
0.04	1.7125	0.0134	127.870	45.844	78.505	6°	0.02396
0.05	1.7696	0.0113	157.051	40.424	71.535	6°	0.03252

Since the the optimum $(C_L/C_D)_c$ is at C_μ of 0.03 for all Reynolds number. The interest and discussion will be focused on the C_μ of 0.03 and the AoA from 0° to 14°. Fig. 4 shows the that the lift reduction for Reynolds number from 4.1×10^6 to 0.18×10^6 is about 3.86%, the lift reduction for Reynolds number from 4.1×10^6 to 2.6×10^6 is less than 1%. However, the drag coefficient is increased by 39.0% for Reynolds number from 4.1×10^6 to 0.18×10^6, and is increased only by 4% for Reynolds number of 2.6×10^6. The substantial drag increase at low Reynolds number is due to the increase of viscous drag.

Table. 6 is the lift and drag force breakdowns with the contributions of pressure, surface viscous friction, and jet reactionary force. C_{LP} and C_{LV} are the pressure and viscous contribution to lift, C_{DP} and C_{DV} are pressure and viscous contribution to drag, F_x and F_y are the jet reactionary force contribution to the drag and lift. Table. 6 indicates that when the Reynolds number is decreased from 4.1×10^6 to 0.18×10^6, the most significant change is the viscous friction drag contribution C_{DV}, which is increased by 66.2%.

Table 6: Detailed force breakdown for the 2D CFJ airfoil at different Reynolds number.

Dimension	Re	AoA	C_L	C_D	C_M	C_{LP}	C_{LV}	C_{DP}	C_{DV}	F_x	F_y
2D	4.1×10^6	6°	1.704	0.012	-0.194	1.9369	0.000446	0.0515	0.00663	-0.0459	-0.233
2D	2.6×10^6	6°	1.693	0.013	-0.193	1.9258	-0.000506	0.0520	0.00708	-0.0463	-0.233
2D	0.18×10^6	6°	1.617	0.017	-0.181	1.8510	0.001382	0.0542	0.01102	-0.0485	-0.235

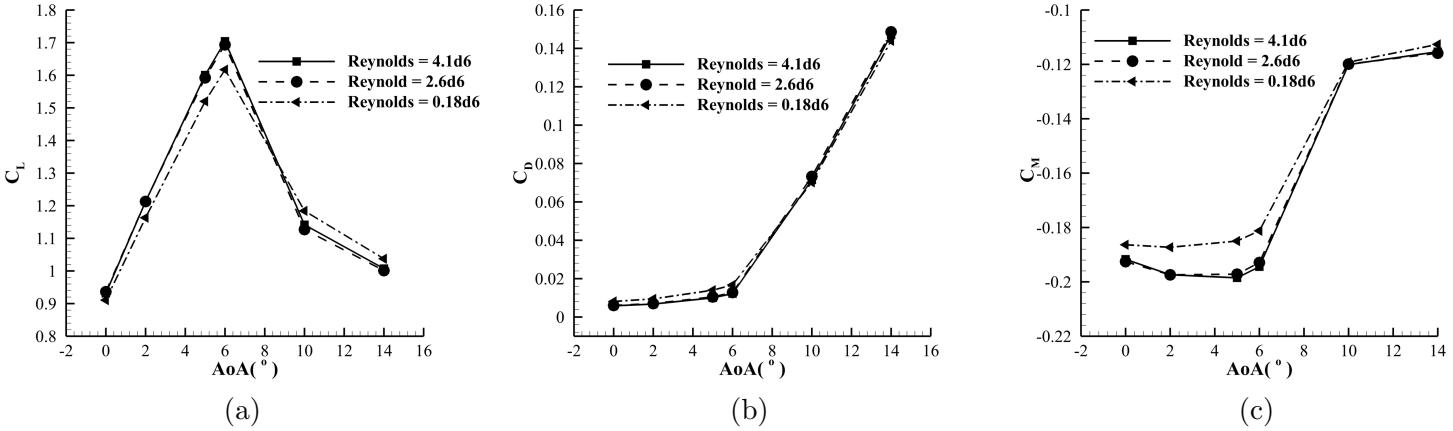

Figure 4: Lift, drag and moment coefficients for the CFJ airfoil at different Reynolds numbers.

Fig. 5 shows that the aerodynamic efficiency, corrected CFJ aerodynamic efficiency, and CFJ productivity efficiency for Reynolds number of 0.18×10^6 has a 31%, 40%, and 42% reduction respectively compared with the case of Reynolds number of 4.1×10^6.

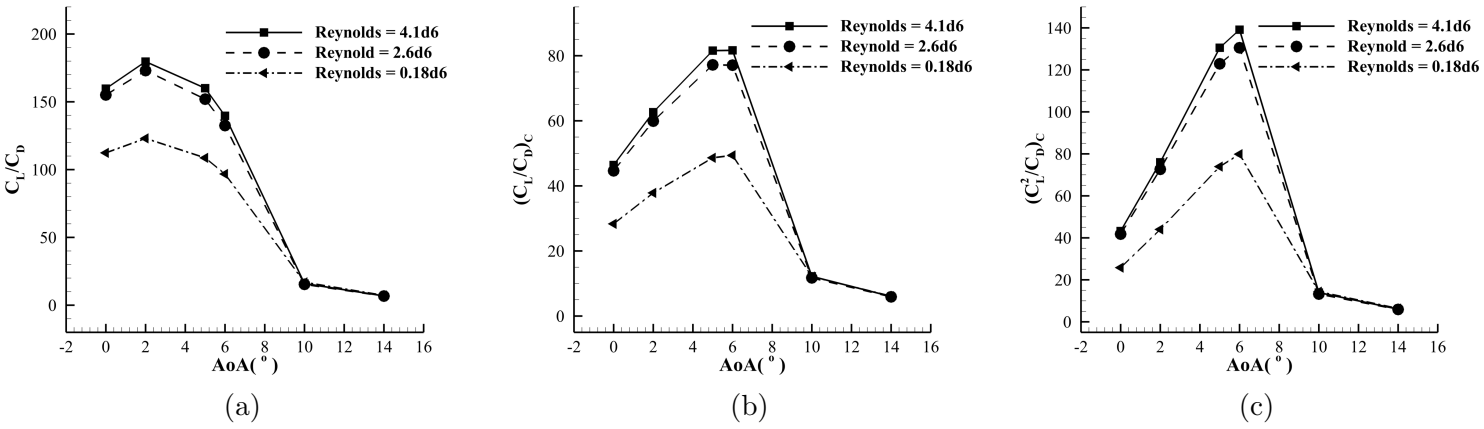

Figure 5: C_L/C_D, $(C_L/C_D)_c$, $(C_L{}^2/C_D)_c$ VS AoA for the CFJ airfoil at different Reynolds numbers.

Fig. 6 shows that for the CFJ airfoil at low Reynolds number, the injection total pressure is increased by 6.6% in order to reach the same C_μ. However, the suction static pressure is not decreased as much, only about 2.3% at AoA of 6°. The CFJ total pressure ratio is increased by 9.1%.

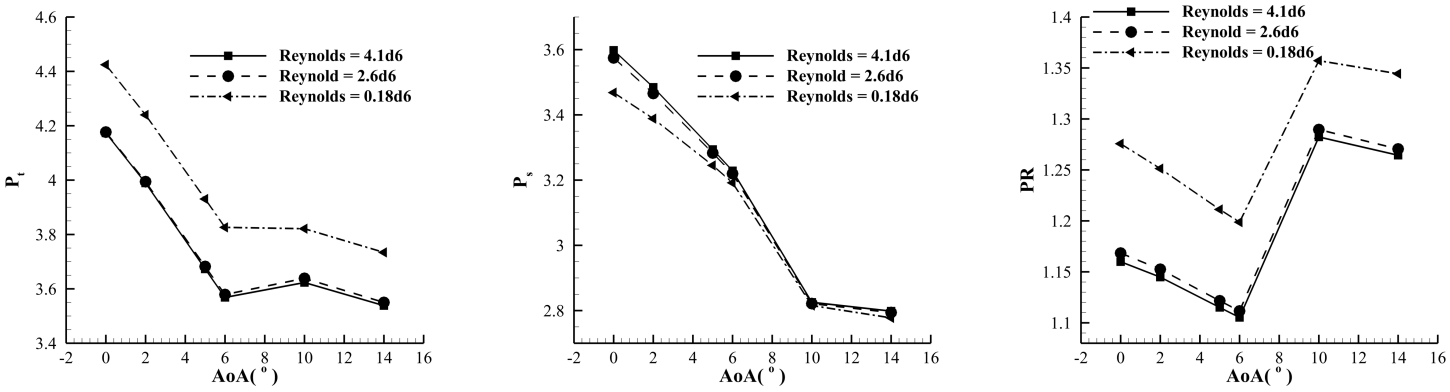

Figure 6: Injection total pressure, Suction static pressure and the total pressure ratio between injection and suction plots for CFJ airfoil at different Reynolds numbers.

Fig. 7 shows that the power coefficient is increased by 75% for Reynolds number of 0.18×10^6. This is mostly because the pressure ratio is substantially increased as shown in Fig. 6. The injection total pressure is increased which caused the injection velocity increases as well under the same static pressure.

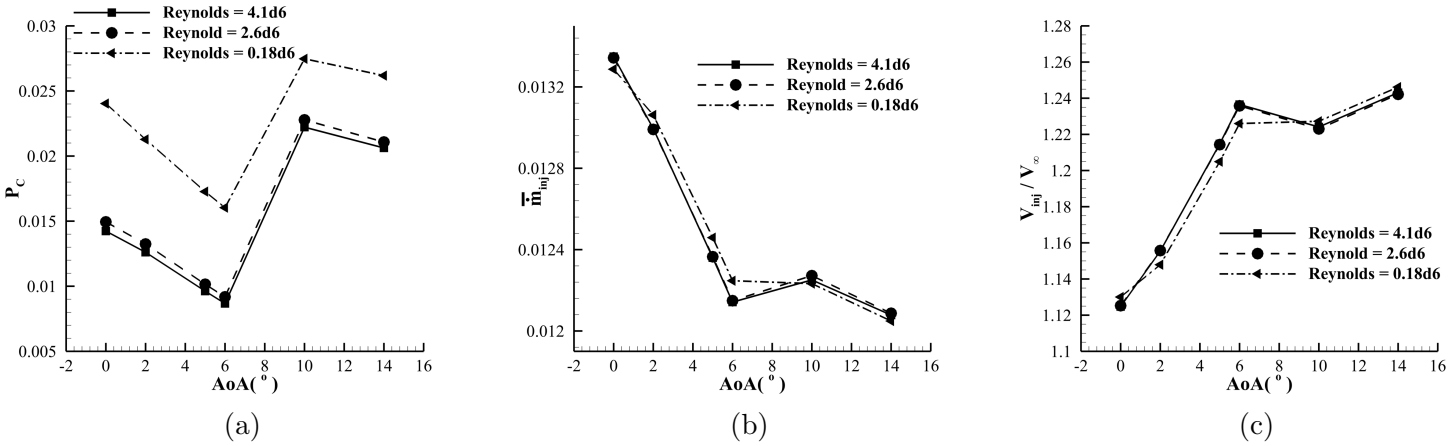

Figure 7: CFJ Power coefficient, Normalized mass flow rate and injection velocity VS *AoA* for the CFJ airfoil at different Reynolds numbers.

Fig. 8 shows the Mach number contours of the flow field for different Reynolds numbers at *AoA* of 6°. Qualitatively, they do not look very different. But quantitatively, Fig. 5 - 7 show that the CFJ airfoil at the low Reynolds number suffers higher viscous loss and higher CFJ pressure ratio and power.

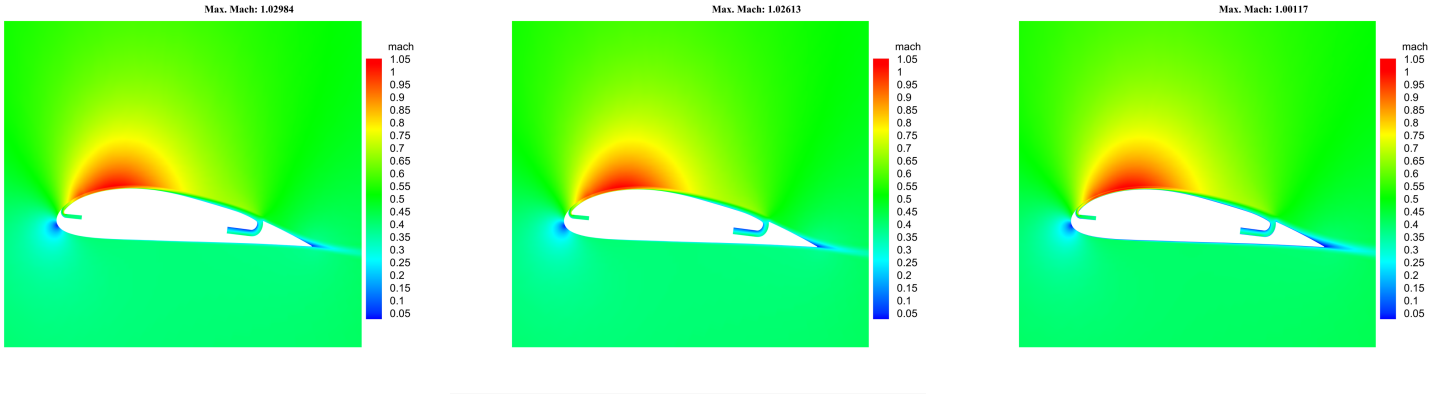

(a) Re $= 4.1 \times 10^6$ (b) Re $= 2.6 \times 10^6$ (c)Re $= 0.18 \times 10^6$

Figure 8: Mach contour plots for CFJ airfoil at different Reynolds numbers.

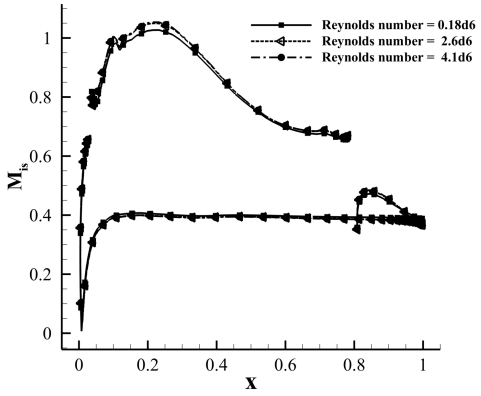

Figure 9: Isentropic Mach number for differnet Reynolds number.

Fig. 9 is the airfoil surface isentropic Mach number distributions at AoA=6° for the different Reynolds number. The difference is not very large as indicated by the lift coefficients in Fig. 4.

6 3D CFJ Wing at Different Reynolds Number

To study the tip vortex effect of 3D wing at different Reynolds numbers, a 3D wing is stacked using the same 2D CFJ airfoil in the last section. The aspect ratio is 20. The Mach number is still 0.46 and the Reynolds numbers are the same as the 2D cases.

When the AoA varies at cruise, it is advantageous to hold the injection total pressure constant as the control law for the micro-compressor [30]. This section hence simulates the CFJ wings performance at cruise condition with the injection total pressure held as constant. The total pressure value fixed is the one at the optimum aerodynamic efficiency point at AoA of 5° for all different Reynolds numbers with C_μ of 0.03. Since the injection total pressure is constant, the C_μ will vary at different AoA.

The P_c and C_μ plots for the CFJ wings at the fixed injection total pressure are shown in Fig. 10. Different from the constant C_μ cases shown in Fig. 7, both the P_c and C_μ have very low value at low AoA and are linearly increased with the AoA even when the airfoil is stalled.

There are two reasons that the power coefficient P_c is increased with the AoA when the injection total pressure is held as constant. First, the mass flow rate is increased due to the leading edge suction pressure decrease. The increased mass flow increases the power coefficient as shown in Eq. (7) and Eq. (8). Second, the total pressure ratio loss is increased when the AoA is increased since the injection velocity is higher and the boundary layer goes through more diffusion before going into the suction duct. With a lower suction total pressure, the pressure ratio is higher to reach the same injection total pressure, the power coefficient is thus increased. Fig. 10 also indicates that the CFJ power coefficient is higher at the low Reynolds number for the same reason explained for the 2D case, which is that the higher viscous loss due to low Reynolds number requires more power to keep the same C_μ.

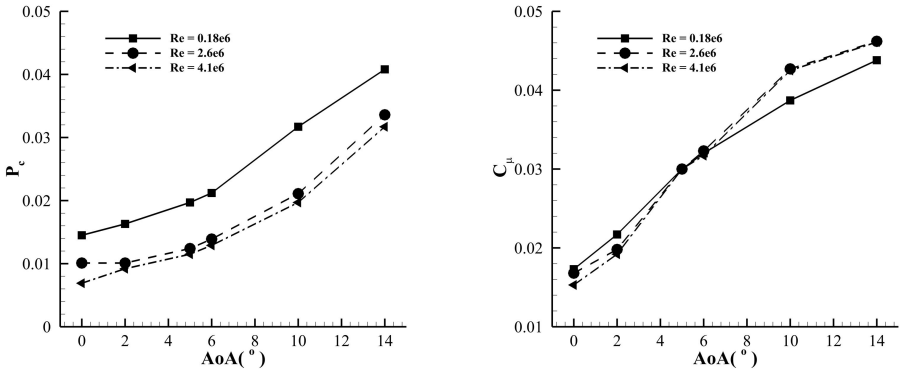

Figure 10: P_c and C_μ plots for CFJ Wings at different Reynolds number and at $M_\infty = 0.46$.

As shown in Fig. 11 (a), away from AoA of 4°, the injection mass flow rate is slightly affected by the Reynolds number, so is the injection jet velocity as shown in Fig. 11 (b).

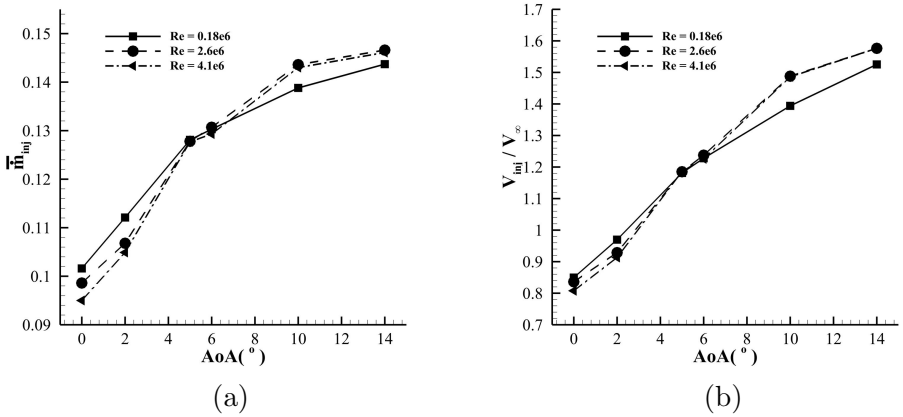

Figure 11: Normalized injection mass flow rate $\overline{\dot{m}}_{inj}$ and $\overline{V}_{inj}$ plots for CFJ Wing at different Reynolds number.

The lift, drag and moment coefficient vs. AoA for the CFJ wing at a fixed injection total pressure at different Reynolds number are shown in Fig. 12. At the low Reynolds number, the maximum C_L drops significantly at AoA of 10°. The drag coefficient C_D at the low Reynolds number is increased across the whole profile as in the 2D case due to the increased viscous drag (Fig. 12 (b)). Since the total pressure is fixed, which allows C_μ varies by its iterations. The stall AoA is about 10°, higher than the 2D cases.

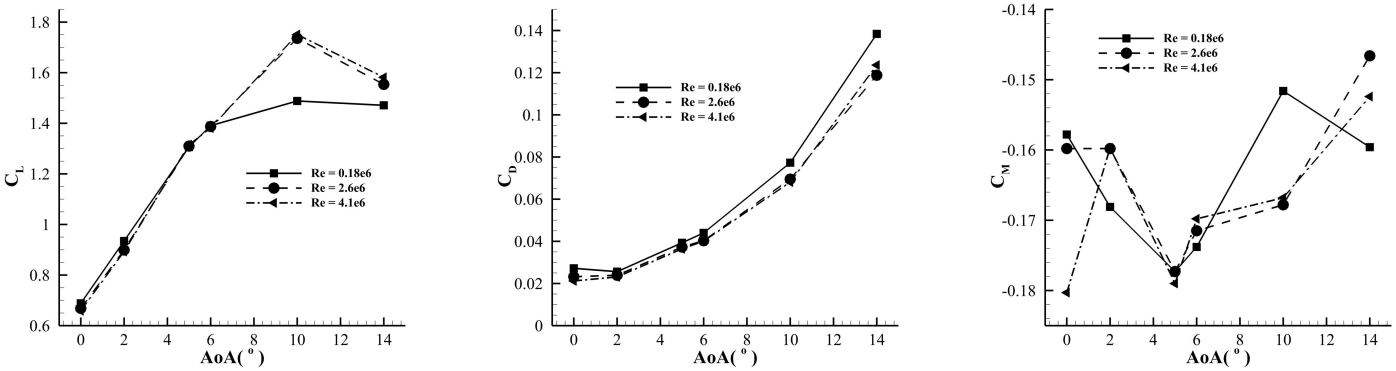

(a) (b) (c)

Figure 12: Lift, drag and moment coefficients for CFJ airfoil at different Reynolds number.

The C_L/C_D, $(C_L/C_D)_c$, $(C_L{}^2/C_D)_c$ at different Reynolds number for the CFJ wing are shown in Fig. 13. The low Reynolds number case has the substantially reduced efficiency for all the AoA as in the 2D cases. As shown in Fig. 13 (a), all the peak C_L/C_D occurs at AoA of 2°. However, the peak $(C_L/C_D)_c$ occurs has a plateau between AoA of 2° and 6°. That is the advantage of holding the injection total pressure constant as indicated by Wang and Zha [30]. The productivity efficiency has a plateau between AoA of 4° and 10° for the high Reynolds number cases. For the low Reynolds number case, the productivity efficiency drops sharply at AoA greater than 6°.

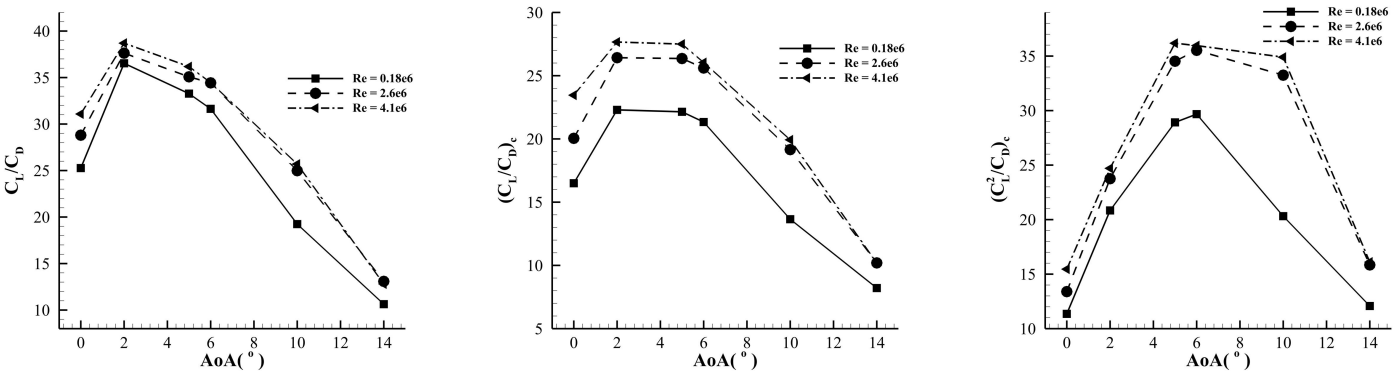

(a) (b) (c)

Figure 13: C_L/C_D, $(C_L/C_D)_c$, $(C_L{}^2/C_D)_c$ plots for CFJ airfoil at different Reynolds number.

Fig. 14 (a) shows the suction static pressure versus AoA at different Reynolds numbers. The injection total pressure are 4.07, 3.87, and 3.84 for Reynolds number of 0.18×10^6, 2.6×10^6, and 4.1×10^6 respectively, which decreases when the Reynolds number increases. Fig. 14 (b) shows the pressure ratio, with the decrease of the

Reynolds number, the PR increases due to more viscous loss.

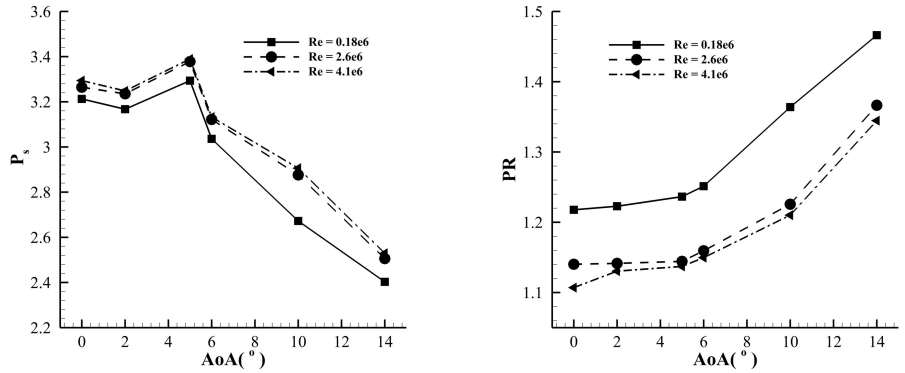

Figure 14: Pt and PR plots for CFJ airfoil at different Reynolds number.

Fig. 15 shows the Isentropic Mach number distribution of the wing section from the wing root to tip at different span locations. At the outer span close to the wing tip, the loading is decreased due to wing tip vortices. The Isentropic Mach number distribution are similar for different Reynolds numbers.

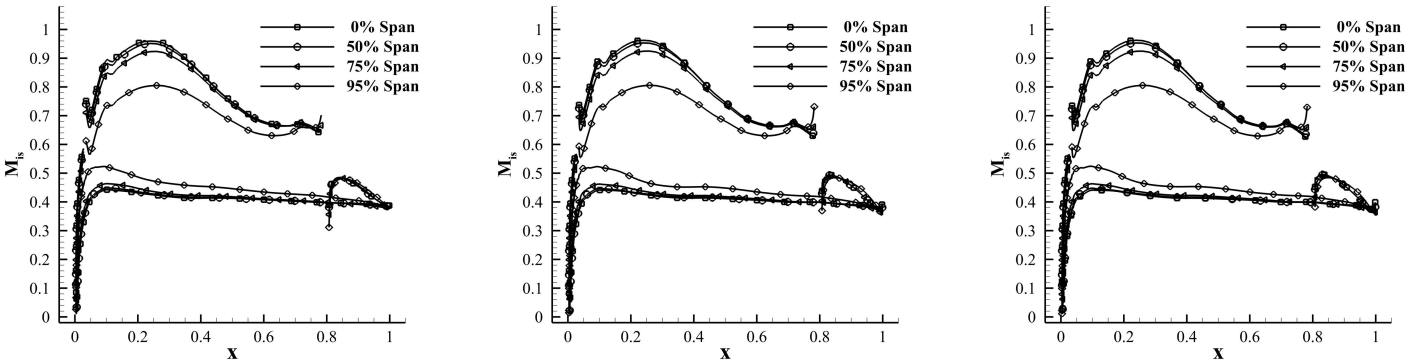

Figure 15: Isentropic Mach Number distributions for the 3D CFJ wings at different Reynolds number at M_∞ of 0.46 and AoA of 5°.

Fig. 16 shows the Mach contours at 10%, 50%, 75% and 95% spanwise location for the CFJ wing at different Reynolds numbers, $AoA = 5°$, $M_\infty = 0.46$. The loading decreases toward the tip. Similar to the 2D case, the flow fields look qualitatively very similar for the different Reynolds numbers, but the drag and energy loss is significantly more for the low Reynolds number case.

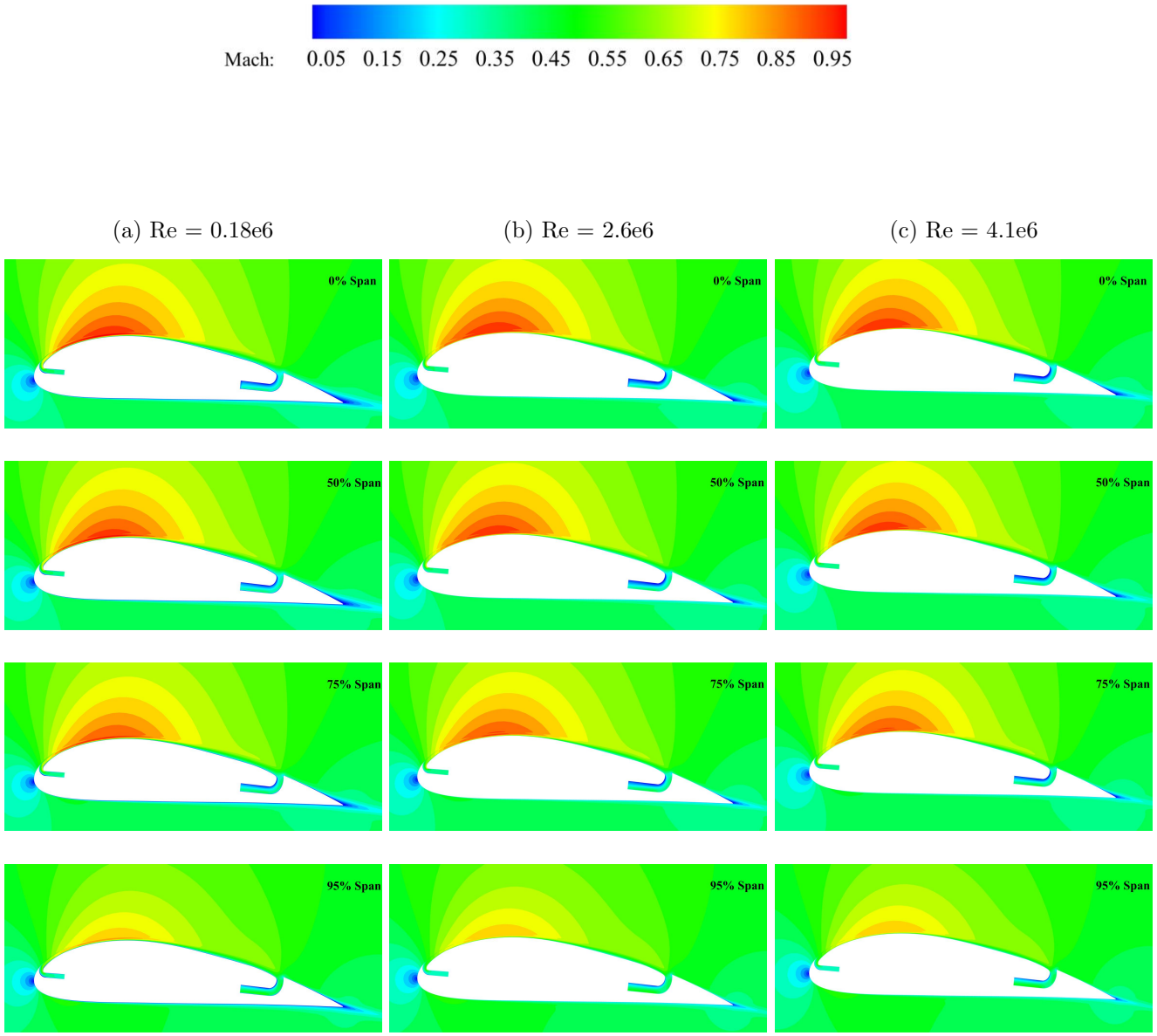

Figure 16: Mach contours at 10%, 50%, 75% and 95% spanwise location for the CFJ wing at different Reynolds numbers, and at $AoA = 5°$, $M_\infty = 0.46$.

7 Conclusion

This paper numerically studies the Reynolds number effect for a 2D Co-Flow Jet (CFJ) airfoil and a 3D wing at freestream Mach number of 0.46. The Reynolds averaged Navier-Stokes equations solver with Spalart-Allmaras turbulence model is utilized for the simulation. The Reynolds number is decreased from 4.1×10^6 to 0.18×10^6 to mimic the altitude change from 10000m to 30000m. The results show that, at Reynolds number of 4.1×10^6, the

best CFJ airfoil corrected aerodynamic efficiency ($(C_L/C_D)_c$) of 81.64 occurs at C_μ of 0.03 at AoA of 6°. When the Reynolds number is reduced to 0.18×10^6, the $(C_L/C_D)_c$ has a 39.5% decrease. It is observed that the reason is due to the dramatic increase of the viscous drag by 66.2% when the Reynolds number is decreased. However, the lift coefficient drops only by 5.1%. The second reason for the decrease of the CFJ airfoil corrected aerodynamic efficiency is that the power coefficient Pc is increased significantly with the decrease of the Reynolds number. It is caused mostly by the increased total pressure ratio of CFJ pumping due to higher loss. The power coefficient is increased by 85% when the Reynolds number is reduced from 4.1×10^6 to 0.18×10^6. The 3D wing with an aspect ratio of 20 based on the same 2D airfoil is also studied for the same Reynolds numbers and freestream Mach number. Similar to the 2D cases, the wing at low Reynolds number suffers significantly increased viscous drag and energy loss of the CFJ.

8 Acknowledgment

The simulations are conducted on Pegasus super computing system at the Center for Computational Sciences at the University of Miami.

Disclosure: The University of Miami and Dr. Gecheng Zha may receive royalties for future commercialization of the intellectual property used in this study.

References

[1] T. Mueller, "Low Reynolds Number Vehicles." AGARDograph No. 288, ISBN 92-835-1486-6, Feb. 1985.

[2] G.-C. Zha and D. C. Paxton, "A Novel Flow Control Method for Airfoil Performance Enhancement Using Co-Flow Jet." *Applications of Circulation Control Technologies*, Chapter 10, p. 293-314, Vol. 214, Progress in Astronautics and Aeronautics, AIAA Book Series, Editors: Joslin, R. D. and Jones, G.S., 2006.

[3] G.-C. Zha, W. Gao, and C. Paxton, "Jet Effects on Co-Flow Jet Airfoil Performance," *AIAA Journal, No. 6,*, vol. 45, pp. 1222–1231, 2007.

[4] G.-C. Zha, C. Paxton, A. Conley, A. Wells, and B. Carroll, "Effect of Injection Slot Size on High Performance Co-Flow Jet Airfoil," *AIAA Journal of Aircraft*, vol. 43, 2006.

[5] G.-C. Zha, B. Carroll, C. Paxton, A. Conley, and A. Wells, "High Performance Airfoil with Co-Flow Jet Flow Control," *AIAA Journal*, vol. 45, 2007.

[6] Wang, B.-Y. and Haddoukessouni, B. and Levy, J. and Zha, G.-C., "Numerical Investigations of Injection Slot Size Effect on the Performance of Co-Flow Jet Airfoil," *Journal of Aircraft*, vol. Vol. 45, No. 6,, pp. pp.2084–2091, 2008.

[7] B. P. E. Dano, D. Kirk, and G.-C. Zha, "Experimental Investigation of Jet Mixing Mechanism of Co- Flow Jet Airfoil." AIAA-2010-4421, 5th AIAA Flow Control Conference, Chicago, IL, 28 Jun - 1 Jul 2010.

[8] B. P. E. Dano, G.-C. Zha, and M. Castillo, "Experimental Study of Co-Flow Jet Airfoil Performance Enhancement Using Micro Discreet Jets." AIAA Paper 2011-0941, 49th AIAA Aerospace Sciences Meeting, Orlando, FL, 4-7 January 2011.

[9] A. Lefebvre, B. Dano, W. Bartow, M. Fronzo, and G. Zha, "Performance and energy expenditure of coflow jet airfoil with variation of mach number," *Journal of Aircraft*, vol. 53, no. 6, pp. 1757–1767, 2016.

[10] A. Lefebvre, G-C. Zha, "Numerical Simulation of Pitching Airfoil Performance Enhancement Using Co-Flow Jet Flow Control," *AIAA paper 2013-2517*, June 2013.

[11] A. Lefebvre, G-C. Zha, "Cow-Flow Jet Airfoil Trade Study Part I : Energy Consumption and Aerodynamic Performance," *32nd AIAA Applied Aerodynamics Conference, AIAA AVIATION Forum, AIAA 2014-2682*, June 2014.

[12] A. Lefebvre, G-C. Zha, "Cow-Flow Jet Airfoil Trade Study Part II : Moment and Drag," *32nd AIAA Applied Aerodynamics Conference, AIAA AVIATION Forum, AIAA 2014-2683*, June 2014.

[13] Lefebvre, A. and Zha, G.-C., "Trade Study of 3D Co-Flow Jet Wing for Cruise Performance." AIAA Paper 2016-0570, AIAA SCITECH2016, AIAA Aerospace Science Meeting, San Diego, CA, 4-8 January 2016.

[14] Lefebvre, A. and Zha, G.-C. , "Design of High Wing Loading Compact Electric Airplane Utilizing Co-Flow Jet Flow Control." AIAA Paper 2015-0772, AIAA SciTech2015: 53nd Aerospace Sciences Meeting, Kissimmee, FL, 5-9 Jan 2015.

[15] Lefebvre, A. and Dano, B. and Bartow, W. and Di Franzo, M. and Zha, G.-C., "Performance Enhancement and Energy Expenditure of Co-Flow Jet Airfoil with Variation of Mach Number." AIAA Paper 2013-0490, AIAA Journal of Aircraft, DOI: 10.2514/1.C033113, 2016.

[16] G.-C. Zha, Y.-C. Yang, Y. Ren, and B. McBreen, "Super-lift and thrusting airfoil of coflow jet-actuated by micro-compressors." AIAA Paper 2017-3061, AIAA AVIATION 2018, Atlanta, GA, Submitted for publication in AIAA Journal , 25 - 29 June 2018.

[17] Yunchao Yang and Gecheng Zha, "Super-Lift Coefficient of Active Flow Control Airfoil: What is the Limit?." AIAA Paper 2017-1693, AIAA SCITECH2017, 55th AIAA Aerospace Science Meeting, Grapevine, January 9-13 2017.

[18] P. R. Spalart and S. R. Allmaras, "A one-equation turbulence model for aerodynamic flows," in *30th Aerospace Sciences Meeting and Exhibit, Aerospace Sciences Meetings, Reno, NV, USA, AIAA Paper 92-0439*, 1992.

[19] Y.-Q. Shen and G.-C. Zha, "Large Eddy Simulation Using a New Set of Sixth Order Schemes for Compressible Viscous Terms ," *Journal of Computational Physics*, vol. 229, pp. 8296–8312, 2010.

[20] Zha, G.C., Shen, Y.Q. and Wang, B.Y., "An improved low diffusion E-CUSP upwind scheme ," *Journal of Computer and Fluids*, vol. 48, pp. 214–220, Sep. 2011.

[21] Y.-Q. Shen and G.-Z. Zha , "Generalized finite compact difference scheme for shock/complex flowfield interaction," *Journal of Computational Physics*, vol. doi:10.1016/j.jcp.2011.01.039, 2011.

[22] Shen, Y.-Q. and Zha, G.-C. and Wang, B.-Y., " Improvement of Stability and Accuracy of Implicit WENO Scheme," *AIAA Journal*, vol. 47, No. 2, pp. 331–344, 2009.

[23] Shen, Y.-Q. and Zha, G.-C. and Chen, X.-Y., " High Order Conservative Differencing for Viscous Terms and the Application to Vortex-Induced Vibration Flows," *Journal of Computational Physics*, vol. 228(2), pp. 8283–8300, 2009.

[24] Shen, Y.-Q. and Zha, G.-C. , " Improvement of the WENO Scheme Smoothness Estimator," *International Journal for Numerical Methods in Fluids*, vol. DOI:10.1002/fld.2186, 2009.

[25] G.-C. Zha and E. Bilgen, "Numerical Study of Three-Dimensional Transonic Flows Using Unfactored Upwind-Relaxation Sweeping Algorithm," *Journal of Computational Physics*, vol. 125, pp. 425–433, 1996.

[26] B.-Y. Wang and G.-C. Zha, "A General Sub-Domain Boundary Mapping Procedure For Structured Grid CFD Parallel Computation," *AIAA Journal of Aerospace Computing, Information, and Communication*, vol. 5, No.11, pp. 2084–2091, 2008.

[27] Y.-Q. Shen, G.-C. Zha, and B.-Y. Wang, "Improvement of Stability and Accuracy of Implicit WENO Scheme ," *AIAA Journal*, vol. 47, pp. 331–344, 2009.

[28] Y. Wang and G.-C. Zha, "Study of 3D Co-flow Jet Wing Induced Drag and Power Consumption at Cruise Conditions." AIAA Paper 2019-0034, AIAA SciTech 2019, San Diego, CA, January 7-11, 2019.

[29] Y. Wang, Y.-C. Yang, and G.-C. Zha, "Study of Super-Lift Coefficient of Co-Flow Jet Airfoil and Its Power Consumption." AIAA Paper 2019-3652, AIAA Aviation 2019, AIAA Applied Aerodynamics Conference, Dallas, Texas, 17-21 June 2019.

[30] Y. Wang and G.-C. Zha, "Study of Mach Number Effect for 2D Co-Flow Jet Airfoil at Cruise Conditions." AIAA Paper 2019-3169, AIAA Aviation 2019, AIAA Applied Aerodynamics Conference, Dallas, Texas, 17-21 June 2019.